Serendipity following attempts to prepare C-doped rutile TiO_2

James A. Sullivan, Elaine M. Neville, Julia Ziegler, J. M. Don MacElroy and K. Ravindranathan Thampi

SFI Strategic Research Cluster in Solar Energy Conversion, UCD School of Chemistry & Chemical Biology, UCD Science Centre, University College Dublin, Belfield, Dublin 4, Ireland Tel: 01 716 2109/2135; E-mail: james.sullivan@ucd.ie elaine.neville@ucd.ie,

Department of Chemistry, University of Hamburg, Martin-Luther-King-Platz 6, Hamburg, Germany E-mail: julia.ziegler@studium.uni-hamburg.de

SFI Strategic Research Cluster in Solar Energy Conversion, UCD School of Chemical and Bioprocess Engineering, University College Dublin, Belfield, Dublin 4, Ireland Tel: 01 716 1995/1824; E-mail: ravindranathan.thampi@ucd.ie, don.macelroy@ucd.ie

Abstract

Attempts to mimic the band gap narrowing seen in anatase TiO_2 following C-doping of the lattice where the C arose from a melamine borate precursor were made in situations where the sol-gel mixture was directed towards rutile formation. The formed materials were characterised using XRD, BET, UV-Vis spectroscopy, XPS and TEM and their activities in promoting the photo-degradation of 4-chlorophenol were analysed. It was found that carbon was not doped into the lattice (in contrast to the situations where the sol-gel mixture was directed towards the precipitation of anatase TiO_2). In spite of how common reports of the preparation of C-doped TiO_2 using sol-gel processes have been, the presence of carbon dopant precursors in a crystallising sol does not necessarily result in the incorporation of C dopants within the final crystalline material, *i.e.* the nature of the condensing sol is also important.

The presence of melamine borate did however increase the proportion of rutile in the final mixture (indeed in the presence of melamine borate the pure rutile phase was formed) and also resulted in materials with higher surface areas (as measured using BET). Furthermore, TEM has shown that rutile TiO_2 condensed in the presence of melamine borate had a much more distinct rod-like shape than that condensed in its absence (the latter being more spherical in shape).

These materials, notwithstanding the absence of any dopant effect, demonstrated enhanced photocatalytic activity when compared with analogous materials prepared in the absence of melamine borate and this effect is ascribed to both their relatively larger surface areas and their specific shape. Therefore, we have serendipitously come across a method for improving the performance of rutile photocatalysts while searching for a method to generate C-doped rutile TiO_2.

Keywords: Rutile TiO_2, photocatalysts, doping.

1 Introduction

TiO_2 is one of the most widely studied and applied semiconductor photocatalysts due to its activity, low cost, photo-stability and non-toxic nature [1, 2]. In recent years TiO_2 has been researched and employed as a photocatalyst in many areas such as wastewater purification[3, 4] and self-cleaning surfaces [5] (*via* organic pollutant oxidation) as well as solar energy conversion [6, 7]. To initiate photocatalysis the semiconductor TiO_2 must first be activated. Energy must be absorbed to promote an electron from the valence band to the conduction band [8]. This generates an electron hole pair, which (if they migrate to the semiconductor surface) may be used in reduction or oxidation (redox) reactions with surface adsorbed species [9].

However, there are difficulties facing the efficiency of TiO_2 as a photocatalyst. Firstly, energy equal to or higher than the band gap of TiO_2 is required for activation[8]. Then, once activated, recombination of generated electron hole pairs must be avoided in order to promote surface redox reactions [10]. Surface area also plays an important role as decreased surface area decreases the concentrations of adsorbed species available for reaction [11].

There are two common crystal phases of TiO_2, *i.e.* anatase and rutile [12]. In general, for photocatalytic processes anatase phase TiO_2 is preferable due to its higher surface area and lower hole electron recombination rates [13]. However, a major limitation associated with the use of anatase TiO_2, particularly as a solar driven photocatalyst, is that the band gap (3.2 eV) [14] is too large for visible light to initiate photocatalysis. Only UV photons with wavelengths below 388 nm can promote electrons and generate active electron hole pairs. One approach which has received a large amount of attention to alter the band gap of TiO_2 and shift towards visible light absorbance is *via* selective doping of metallic and/or non-

metallic elements (such as carbon) into the TiO_2 lattice [15-32]. In general anionic carbide dopants are considered more beneficial than cationic dopants for photocatalytic performance [28].

The eventual nature of C-dopants within TiO_2 lattices has been the subject of much debate and there are several excellent reviews and recent works for example see [33, 34] that discuss their incorporation, their chemical nature and their modes of action. A more extensive discussion of the nature and modes of action of doping and aspects such as the valance induction law and other proposed mechanisms is beyond the scope of this work, given in fact that we failed to generate any doped materials (see later).

Such doping has, in general been applied to the anatase crystal phase of TiO_2 [31]. These techniques for C-doping anatase phase TiO_2, through the addition of C-containing precursors to a sol gel mixture of precipitating TiO_2, are now widespread and considered routine.

Rutile phase TiO_2 has a lower band gap (~3.0 eV) [14] than the anatase phase, and it exhibits lower surface areas and higher hole electron recombination rates. These characteristics, coupled with the (bandgap and non-bandgap related) benefits of C-doping mentioned above, suggest that C-doped rutile should perform more efficiently as a photocatalyst than its undoped analogue. While there are many examples of metal doped rutile systems (in which the metal sits at the Ti site of TiO_2, *e.g.* see [35, 36]) we have not seen any examples of C-doped rutile nanoparticles, although theoretical discussions of such systems have been noted [37] and carbon-doped thin films in the rutile phase (produced by heating Ti metal in a CH_4 flame) [18] have also been formed. The paucity of these reports is surprising, given the

abundant, relatively facile techniques available for introducing C dopants into an anatase lattice.

In this work we have attempted to form nanoparticles of C-doped TiO_2 in the rutile phase in order to determine whether its characteristics as a photocatalyst are affected in the same way as those of anatase following the addition of a dopant-containing solution to the crystallising sol. We have endeavoured to add carbon to the rutile TiO_2 lattice with a technique which we have previously used to reproducibly form the doped anatase analogue [29].

Typically in low temperature solution-phase synthesis of TiO_2 the anatase phase is favoured, due to precursor chemistry and surface energies [41]. In small crystallites, particle surface energy makes up a large part of the total energy of the crystal. It has been found that anatase has a lower surface energy than rutile [42] and so this favours the formation of anatase phase crystals. However, as the crystals increase in size (*e.g. via* sintering) surface energy plays a lesser role in the total crystal energy, a phase crossover occurs, and rutile crystals become more stable than anatase phase crystals, at about 30 nm [40]. Consequently, rutile (the thermodynamically more stable phase [41]) can be formed when anatase is calcined at high temperature (above 800 °C) and small crystallites sinter into larger particles. In order to retain dopants such as carbon in TiO_2, as well as to retain small particle sizes (with large surface area), a low temperature synthesis is required.

Low temperature synthesis of rutile phase TiO_2 nanocrystals can be challenging and various methods have been studied such as addition of mineral additives [42] or rutile seed crystals [43] in order to promote rutile formation. However, these methods have certain disadvantages [44] such as contamination and phase impurity. Another possible approach involves varying

synthesis conditions in order to affect the rates of both hydrolysis of the Ti precursor and condensation [12] of the pre- TiO_2 sol, which in turn affects crystal formation.

In acidic conditions, using certain precursors, hydrolysis can be promoted and the rate of condensation decreased [45, 46]. This allows all of the hydrolysis steps to complete before condensation steps begin and results in the thermodynamically stable rutile phase being formed [47]. It is known that the presence of nitric acid, which may also form NO_2 in the gas phase, increases the possibility of forming rutile at lower temperatures [48]. Conversely, in neutral or basic conditions, precursor hydrolysis steps can be slowed and condensation can begin before hydrolysis is completed. This results in the formation of the metastable anatase phase or in the formation of amorphous TiO_2 [47].

Another method for the formation of rutile nanocrystals at low temperature is *via* acidic low temperature hydrothermal treatment of an amorphous TiO_2 precursor [38, 49]. This method produces rutile *via* a dissolution–precipitation mechanism which depends on reactant interactions (*e.g.* addition of HCl) in conjunction with hydrothermal conditions that crystallize the amorphous TiO_2 under pressure [50-53]. Note again that acidic conditions are required.

Here, we have used two modified low temperature methods previously reported [38, 45] in attempts to synthesise rutile phase C-doped TiO_2 nanoparticles. The first approach involved the addition of nitric acid to hydrolyse a Ti precursor. The second approach entailed autoclaving (under acidic conditions) amorphous TiO_2. In both cases, carbon doping was attempted using the addition of melamine borate to the pre-TiO_2 sol. Addition of solutions of this material to the crystallising sol has been previously found to be a facile, reliable,

reproducible and cost-effective way to introduce dopant levels of C atoms into the anatase TiO_2 structure [29]. Once formed, the materials were characterized using a range of physical techniques such as diffuse reflectance UV-Vis spectroscopy, X-ray diffraction, X-ray photoelectron spectroscopy, Transmission Electron Microscopy and N_2 physisorption. Photocatalytic activities under visible light were investigated using the oxidation of 4-chlorophenol as a model reaction.

As it happened, none of these proposed techniques for incorporating any form of C-dopant within the lattice of a rutile TiO_2 sample proved effective and in all cases the materials remained undoped. However, as a pleasant surprise, the materials formed following these attempts to dope, were more phase-pure than the nominally un-doped analogues and were also significantly more active photo-catalysts. In brief, our attempts to dope have, by a happy accident, led to the development of more active rutile photo-catalysts.

2 Experimental

Rutile phase TiO_2 was formed using two modified low temperature methods outlined below. Carbon doping was attempted using the addition of melamine borate as a source of carbon dopant. P25 (Degussa) and Rutile nanopowder (99.5%, Aldrich) were used as reference materials.

2.1 Preparation of rutile TiO_2 using a nitric acid (HNO_3) method

TiO_2 (TiO_2 (HNO_3)) was formed using a method outlined by Tang *et al.* involving the hydrolysis of titanium (IV) butoxide with an aqueous solution of nitric acid [45]. At room

temperature 43 mL titanium (IV) butoxide (97%, Aldrich) was added to a stirred solution of 113 mL deionised water and 16.5 mL nitric acid (69 %, Riedel-de Haen). Two layers formed. The upper organic layer was yellow and contained butanol which was formed during the hydrolysis. The lower aqueous layer was the pre-TiO_2 transparent sol. This layer was separated and heated slowly without stirring to 45 °C. The solution was stored at 50 °C in the oven and became turbid after 1 h. After 3 h a white powder formed. After 24 h the solution was decanted and the wet powder obtained was dried at 50 °C and ground with a pestle and mortar. The powder was washed with water and centrifuged (to remove traces of nitrate), dried at 50 °C, ground and calcined at 400 °C for 2 hours.

Attempts to form carbon-doped rutile phase TiO_2 (C-TiO_2 (HNO_3)) were carried out in the same manner (using Ti:HNO_3:H_2O 1:2:50) but with the addition of melamine borate. A saturated solution of melamine borate was formed by adding 3.4 g of melamine borate (Budenheim) to 0.5 L of deionised water under constant stirring at room temperature. After 24 h, the solution was filtered through Whatman Grade 1 filter paper. 17.6 mL of this aqueous melamine borate solution was added to the pre-TiO_2 aqueous solution after separation from the organic layer (see synthesis of TiO_2 (HNO_3) above).

2.2 Rutile TiO_2 using an autoclave (AC) method

Rutile phase TiO_2 (TiO_2 (AC)) was also prepared using the following method (Reyes-Coronado *et al.*) at low pH and under autoclave conditions [38]. First titanium isopropoxide (97%, Aldrich) was hydrolysed in a solution of 2-propanol (99 %) and deionised water (1 %). Typically an ice-cooled solution of 110 mL of deionised water and 1050 mL 2-propanol (Sigma-Aldrich) was added to a stirred solution of 50 mL titanium (IV) isopropoxide (97%,

Aldrich) and 1050 mL 2-propanol in an ice bath. Afterwards, the clear solution was stirred at room temperature for 24 h. During this time the solution became turbid and white. After filtration a solid precipitate (amorphous TiO_2) was obtained and dried at room temperature. The amorphous TiO_2 was then dissolved in 3 M HCl which was subsequently diluted to 0.3 M in a Teflon cup. The Teflon cup was placed in an autoclave and was heated for eight hours at 200 °C. After this, the solution was filtered and a grey solid was obtained. The powder was then calcined at 400 °C for 2 hours.

Attempts to synthesise carbon-doped rutile TiO_2 (C-TiO_2 (AC)) followed the same method but with the addition of melamine borate to the pre-TiO_2 sol. 12 mL of saturated aqueous melamine borate solution substituted 12 mL of deionised water in the pre-TiO_2 solution.

2.3 Characterisations

Powder XRD patterns were collected using a Siemens D500 Kristalloflex using Cu Kα radiation. N_2 physisorption isotherms were collected on a Quantachrome Nova 2000e. Diffuse Reflectance UV-Vis spectroscopy (DRS) was carried out using an Analytik Jena Specord 210 spectrometer equipped with an integrating sphere attachment for measurement of spectra from powder samples. X-ray Photoelectron Spectroscopy (XPS) was carried out with a Kratos AXIS 165 spectrometer using a monochromatic X-ray source (Al Kα 1486.58 eV). TEM images were measured on a Technai T12 transmission electron microscope.

2.4 Photocatalytic activity measurements

Photocatalytic activity of the materials was tested by investigating the photocatalytic degradation of 4-chlorophenol solutions under visible light irradiation. 80 mg of photocatalyst powder was dispersed in 40 mL of a 0.5 mM solution of 4-chlorophenol. The

mixture was sonicated for 15 min before being purged with air for 5 min. Samples were stirred in the dark for 30 min in order to reach an adsorption – desorption equilibrium. Irradiation was carried out in an Atlas Suntest CPS (AM1.5 G) solar simulator unit with UV filter film ($\lambda > 410$ nm). Samples were extracted hourly for 5 hours and the degradation (complete mineralisation) of 4-chlorophenol was monitored using Total Organic Carbon (TOC) analysis (Shimadzu TOC V-CPH).

3 Results and Discussion.

In the following sections we present the characterisation data of the 4 prepared samples, 2 that nominally should contain C-dopants (if the previously demonstrated method of dopant incorporation operates) and 2 that should be un-doped. It transpires that while there are significant measurable differences, observable using a range of techniques, between the two families of materials (*i.e.* those produced in the presence of melamine borate and those produced in its absence) that there is no actual incorporation of carbon into the rutile lattices. Furthermore, serendipitously, these formed materials were of a different shape and had improved photo-catalytic reactivity when compared to the nominally un-doped materials.

3.1 XRD and physisorption analysis

Materials were analysed using XRD to determine phase composition and crystalline particle sizes. XRD patterns are shown in Figure 1. P25 (Degussa) and Rutile nanopowder (Aldrich) are also shown for comparison. P25 displays a mixture of both anatase phase peaks (JCPDS 21-1272) and rutile phase peaks (JCPDS 21-1276), while the Rutile nanopowder consists of a mainly rutile phase with trace anatase phase peaks. Molar ratios of rutile and anatase were calculated using the intensities of the (101) anatase peak and (110) rutile peak according to

the equations proposed by Spurr *et al.* [54].

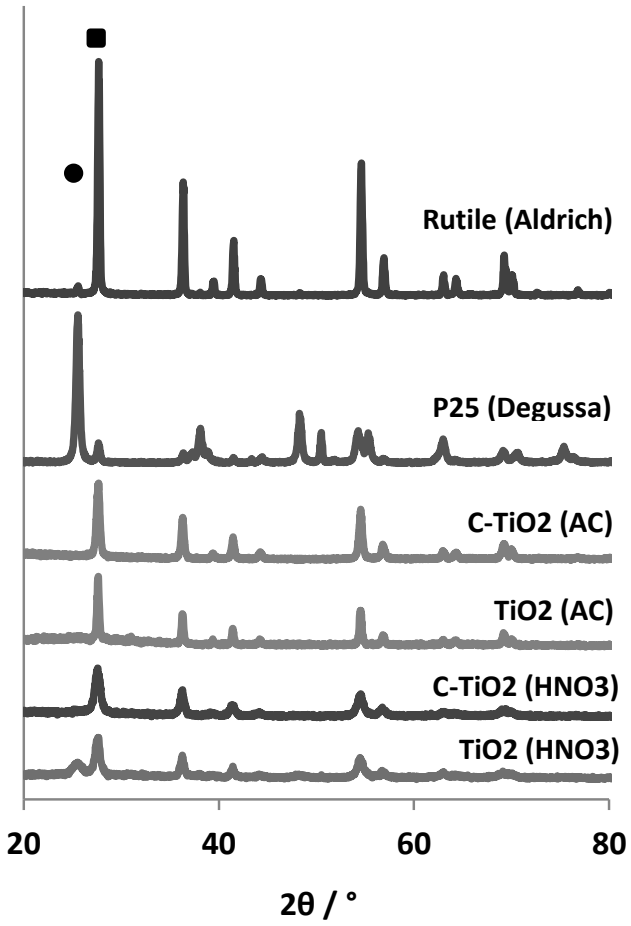

Figure 1. XRD patterns of TiO_2 (HNO_3), C-TiO_2 (HNO_3) TiO_2 (AC), C-TiO_2 (AC), P25 (Degussa) and Rutile nanopowder (Adrich). The (101) anatase peak is indicated by ●, the (110) rutile peak is indicated by ■.

Undoped TiO_2 formed from the nitric acid method (TiO_2 (HNO_3)) was of predominantly rutile phase with small amounts of anatase (86:14 rutile:anatase). TiO_2 formed from the nitric acid method in the presence of a dopant source (C-TiO_2 (HNO_3)) contained only the rutile phase. Similarly, TiO_2 formed from the autoclave method (TiO_2 (AC)) was of predominantly rutile phase composition (99:1 rutile:anatase) while TiO_2 formed from the autoclave method in the presence of melamine borate (C-TiO_2 (AC)) again was a pure rutile phase material.

It seems the addition of melamine borate to the condensing mixture has further promoted the

formation of rutile phase TiO_2. Cationic dopants "within" lattices have previously been reported to promote the formation of rutile [55] though the exact nature of the promotion is unknown but it may be due to disruption of the crystal formation during hydrolysis / condensation, impeding the rate of condensation and thus creating conditions favourable for rutile formation. However, it seems that whatever mechanism proposed by Shirley *et al.* [53] to promote this cannot operate here (since dopants are not incorporated into our final lattices – see later).

TEM (see later) shows that the species precipitated in the absence of melamine borate are approximately spherical and their crystalline particle sizes (as determined using the Scherrer equation [56]) are reported in Table 1. In these calculations the diffraction pattern peaks at (101) anatase peak and (110) rutile peak are utilized. The equation $\tau = K\lambda / \beta\cos\theta$, where K is the shape factor (0.94), λ is the X-ray wavelength, β is the line broadening at half the maximum intensity (FWHM) of the peak, and θ is the Bragg angle (peak position) is used. It should be recalled that the use of this equation assumes that the particles are spherical – a situation that TEM measurements (see later) show not to be the case for the solids condensed in the presence of melamine borate.

N_2 physisorption was carried out in order to determine the surface areas of the materials synthesised. As expected decreasing crystalline particle size resulted in an increased surface area. As presented in Table 1, TiO_2 materials prepared in the presence of melamine borate (C-TiO_2 (HNO_3), C-TiO_2 (AC)) had increased surface areas in comparison to their "pure" equivalents (TiO_2 (HNO_3), TiO_2 (AC)).

3.2 UV-Vis spectroscopy

The materials were analysed using UV-Vis spectroscopy. Figure 2 shows the UV-Vis spectra of P25 (Degussa), Rutile nanopowder (Aldrich) along with the synthesised TiO_2 (HNO_3), C-TiO_2 (HNO_3), TiO_2 (AC) and C- TiO_2 (AC). The materials synthesised *via* the nitric acid method, TiO_2 (HNO_3) and C-TiO_2 (HNO_3), were white in colour while those synthesised *via* the autoclave method, TiO_2 (AC) and C- TiO_2 (AC), were slightly grey in colour. This is reflected in different absorptions in the visible region of the spectra (400 nm onwards).

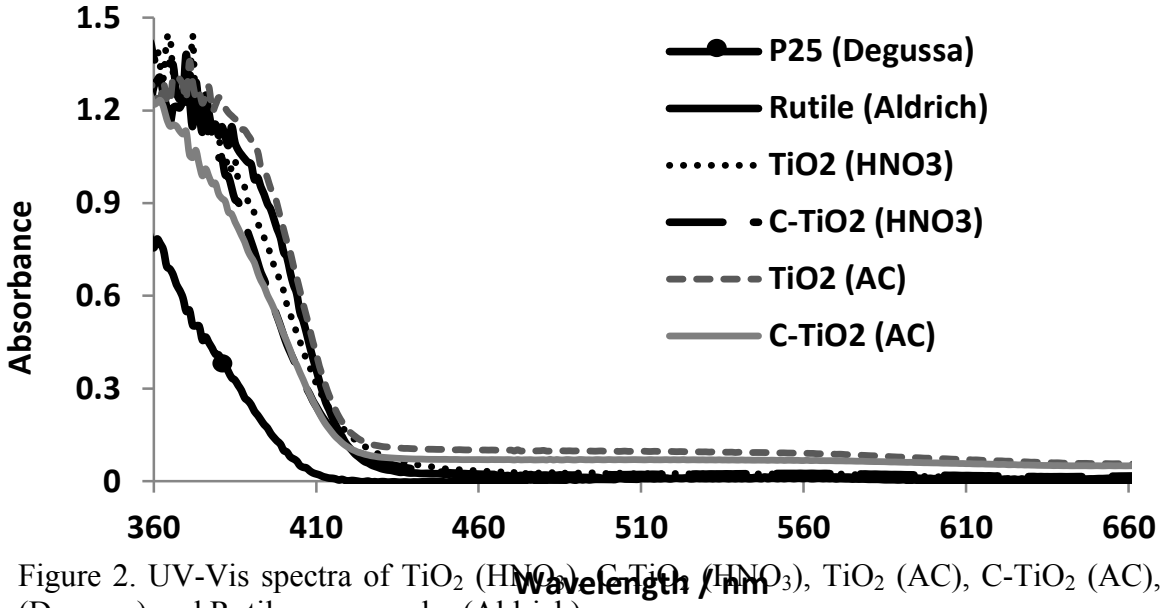

Figure 2. UV-Vis spectra of TiO_2 (HNO_3), C-TiO_2 (HNO_3), TiO_2 (AC), C-TiO_2 (AC), P25 (Degussa) and Rutile nanopowder (Aldrich)

As expected the high energy feature absorbance onsets of the predominantly rutile materials was shifted further towards the visible region (~ 420 nm) compared to the mainly anatase phase P25 (~410 nm). The spectra of the 3 nominally doped and un-doped rutile materials were all comparable to one another. Absorbance onsets were estimated by drawing a tangent to the high-energy feature of the UV-Vis spectrum and approximating the wavelength at which the tangent intercepts a line with an absorbance value of zero.

Absorption coefficients were used to estimate the bandgaps of the various materials according to the Tauc equation $\alpha h\nu = B(h\nu - E_g)^n$ where α is the absorption coefficient, $h\nu$ is the photon energy, B is a constant, E_g is the band gap and n = 0.5 for direct band gaps and n = 2 for indirect band gaps [57]. The intercept of the extrapolated linear region of plots of $(\alpha h\nu)^n$ versus energy ($h\nu$) on the energy axis gave the material band gap [58]. Calculated values for both direct and indirect band gaps are given, Table 2.

A decrease in band gap is observed in the rutile phase materials as compared to the mainly anatase phase P25 TiO_2. However, no substantial change in band gap is observed for the materials that had melamine borate incorporated within the preparation mixture.

Both of the materials synthesised *via* autoclaving (TiO_2 (AC) and C-TiO_2 (AC)) showed increased absorbance across the visible region (at $\lambda > 420$ nm) owing to their slightly greyish colour even following calcination.

In any case, regarding the substantive issue, these results (which suggest no change to the opto-electronic properties of the materials crystallised in the presence of melamine borate) is a significant difference to those observed when anatase TiO_2 is condensed in the presence of melamine borate using a sol-gel process. In the latter materials the presence of melamine borate results in the incorporation of C atoms into the lattice and a subsequent decrease in the electronic bandgap [29] that is reflected by a yellow colour in the material. This result suggests that the extent of any doping of these rutile materials was minimal.

3.3 XPS measurements

X-ray photoelectron spectroscopy (XPS) was carried out to determine whether in fact there were dopants contained within the relevant materials. The C 1s regions of the XPS profiles of TiO_2 (HNO_3), C-TiO_2 (HNO_3), TiO_2 (AC) and C-TiO_2 (AC) were studied. Initially in all samples three peaks were seen at binding energies of ~285, ~286 and ~289 eV. The peak at 285eV is an instrumental artefact related to elemental adventitious carbon [59] present in all XPS measurements. The peaks at 286 and 289 eV have previously been related in the literature to interstitial carbonate dopants as well as oxidised carbon species adsorbed on the surface of the material [21, 43, 60-63]. However these peaks were found to be present in both the doped and un-doped samples and must be related to carbon contaminants on the surface of the samples. A peak at 282 eV related to Ti-C, or carbon substitutionally doped in the place of oxygen in the TiO_2 lattice [17] was not observed in any of the samples. This peak has been seen in the analogous anatase materials [29].

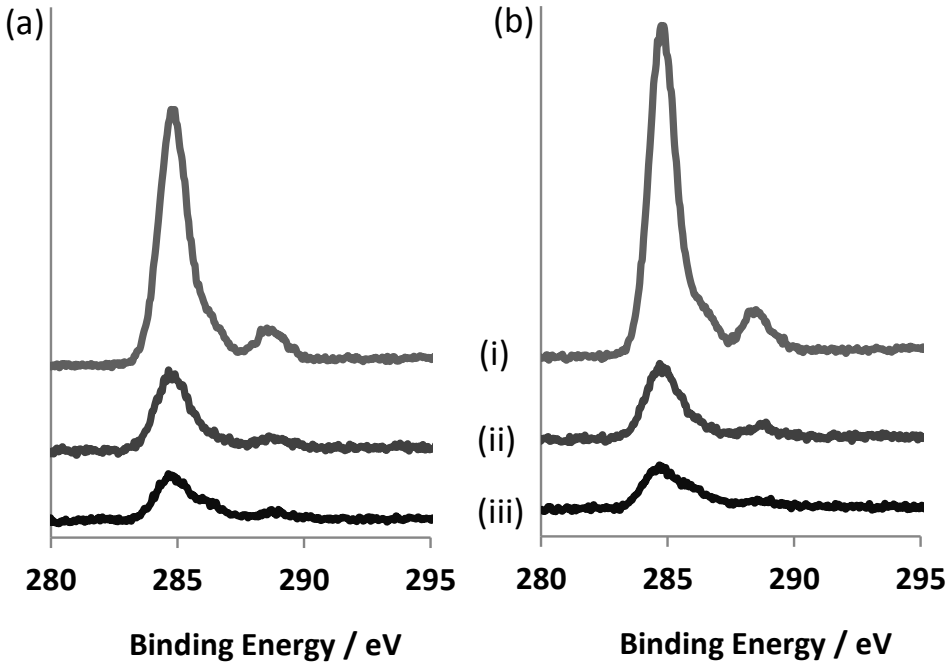

Figure 3. XPS C 1s peaks of (a) C-TiO_2 (HNO_3) and (b) C-TiO_2 (AC), (i) before sputtering, (ii) after sputtering with 2 keV Ar^+ ions for 8 min and (iii) after sputtering with 2 keV Ar^+ ions for 8 min and 4 keV Ar^+ ions for 5 min. Note: no peak appears at 282 eV before or after sputtering.

XPS analysis of C-TiO_2 (HNO_3) and C-TiO_2 (AC) was also carried out after sputtering samples for 8 min with low energy Ar ions (2 keV) followed directly by sputtering for 5 min with high energy Ar ions (4 keV). The purpose of this treatment was to etch away the top surface layers of the material. This would remove any adsorbed carbonate species that may be masking at peak at 282 eV related to Ti-C. After sputtering, the peak at 285 eV, *i.e.* the instrumental artefact, remained in the spectra of all samples. The intensity of the C 1s peaks at 286 and 289 eV (relating to carbonate species) decreased continually upon sputtering (Figure 3). In contrast to the situation when the analogous anatase TiO_2 is crystallised in the presence of melamine borate [29], here no new peak at 282 eV relating to Ti-C was revealed.

These XPS results, as well as the UV-Vis derived bandgap measurements above, suggest that there has been no incorporation of C dopant into the rutile phase TiO_2, *i.e.* these attempts to incorporate dopant carbon into the rutile phase of TiO_2 were not successful. This is in stark contrast to the situation when TiO_2 is allowed to crystallise in its anatase form in the presence of melamine borate where decreased bandgaps were noted in the UV-Vis spectra and dopant C was found in the XPS. This in turn suggests that the incorporation of the C-dopant is not a straightforward process and that aspects of the preparation including pH (the major difference between these two preparations) have an important role to play in the eventual doping. It is emphasized that in spite of the presence of nitrogen in melamine borate, doping of N atoms was never detected in any samples, irrespective of the final TiO_2 crystalline phases [17, 29, 30].

3.4 TEM measurements

Transmission Electron Micrographs of the nominally doped and undoped samples prepared using both techniques are shown in figure 4. Images of the samples prepared in the absence

of melamine are comparable to those seem previously [38, 45]. Tang *et al.* [45] and Oskam *et al.* [38] have also reported approximately spherical particles following the HNO_3 and AC methods we have employed. The TiO_2 particles produced using the AC methods are reported to form rods if the autothermal treatment is allowed to continue beyond 20 h.

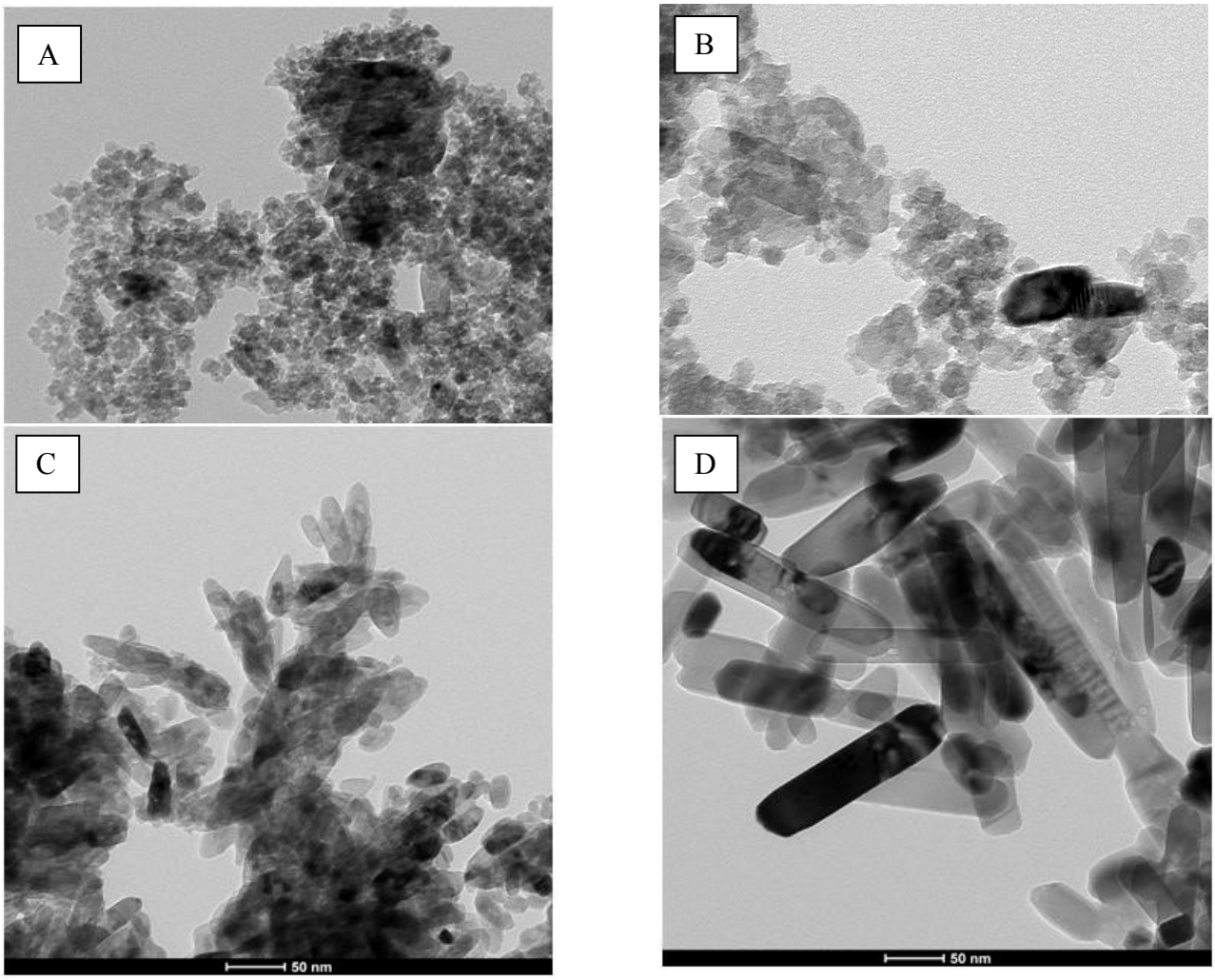

Figure 4 TEM images of the rutile TiO_2 produced by the HNO_3 method (left panels (A and C)) and the autoclave method (right panels (B and D)) formed in the absence (upper panels (A and B)) and presence (lower panels (C and D)) of melamine borate in the synthesis mixture.

In this work the particles produced in the presence of melamine borate have a much more defined rod-like shape. This is more obvious in the samples produced using the AC method (bottom right panel) than those produced using the HNO_3 method (bottom left panel).

The rod-like particles produced in the presence of melamine borate using HNO_3 method are ~69 ± 14 nm in length and ~30 ± 2 nm in width while in the case of the particles produced in the presence of melamine borate using the autoclave method they are ~183 ± 30 nm in length and ~ 39 ± 5 nm in width. The latter particles also appear more defined than the analogous HNO_3-precipitated materials.

This correlates with the surface areas of the materials as discussed above where the HNO_3-produced materials (which are smaller less defined rods) have a higher surface area (36.5 m^2g^{-1}) than those produced using the AC method (21.0 m^2g^{-1}).

The formation of TiO_2 rods through anisotropic growth of nanocrystals has been noted previously and been ascribed to an oriented attachment process from the forming gel [36, 62]. Another possibility is that preferential growth in 1 dimension over another is facilitated by the action of another species in solution preferentially capping one particular plane thereby forcing growth in another direction [65]. It might be that the melamine borate is acting in this way.

3.5 Photo-catalytic activity measurements

Photo-catalytic activity experiments were carried out using the degradation of 4-chlorophenol under visible light as a model reaction (Figure 5). Previously, using C-doped anatase TiO_2 formed through the addition of melamine borate to the catalyst preparation mixture, we have found improved optical absorbance characteristics that in turn have led to improved reactivity (relative to an undoped analogue) [29]. We have ascribed this to an increased generation of charge carriers and subsequent generation of oxidising species (*e.g.* h^+, OH^-) within the

reaction mixture. We would not expect to find a similar effect here given that C atoms are not incorporated into the TiO_2 and therefore the spectral characteristics of the material are unchanged.

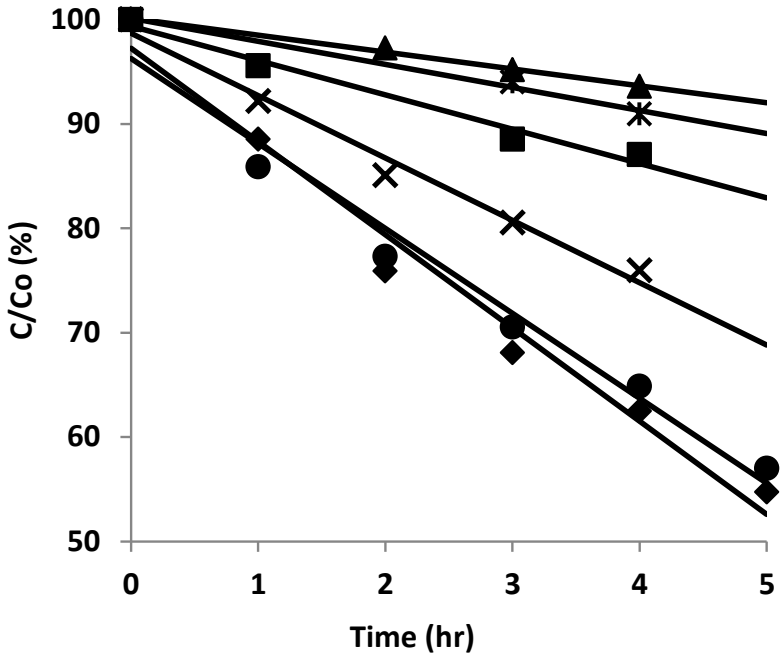

Figure 5. The photocatalytic degradation of 4-chlorophenol under visible light only by TiO_2 (HNO_3) (*), C-TiO_2 (HNO_3) (**X**), TiO_2 (AC) (▲) C-TiO_2 (AC) (●), P25 (Degussa) (♦) and Rutile nanopowder (Aldrich) (■).

Of all the materials tested, P25 TiO_2 performed best, degrading almost 50 % of the 4-chlorophenol in 5 hours (Figure 5) despite having a reduced (but not zero) absorbance in the visible region compared to the rutile materials (Figure 2). This confirms that enhanced light absorbance is only one of many factors that influence photo-catalytic efficiencies of these catalysts. Increased surface area, crystallinity and reduced electron hole recombination (from an optimized anatase:rutile phase composition) also play an important role in producing photo-catalytically active materials.

Regarding the synthesised materials, the activities of the un-doped materials were comparable

to one another (converting ~10% after 5 h of reaction) as were their surface areas and morphologies (as measured using BET and TEM) – see above. The two nominally doped samples removed far more 4-chlorophenol than their un-doped analogues. The C-TiO_2 (AC) catalyst was more active than the C-TiO_2 (HNO_3) with the former converting over 40% during the reaction and the latter converting ~30%.

Since the opto-electronic properties of these materials are unchanged following the preparations in the presence of melamine borate, and there is no evidence for carbon doping, some other effects must be in operation to cause this increased reactivity.

The surface areas of these materials were higher than those of the un-doped analogues and it is probable that this larger surface area contributed to the improved reactivity. However, this cannot be the only influence on the improvement seen in photo-catalysis.

Of these materials the less active C-TiO_2 (HNO_3) sample had the larger surface area (36.5 m^2g^{-1} compared to 21.0 m^2g^{-1} for the AC) and yet this sample (while being more active than the analogous material prepared in the absence of melamine borate) was less active than the C-TiO_2 (AC) photocatalyst.

Thus, it seems that while our initial attempts to form C-doped rutile were a failure, by a happy accident we have come to a method for producing a more phase-pure and reactive rutile material

A possible explanation for this might be found in the TEM analyses of the materials (Figure 4). The AC-produced samples appear far more defined than the HNO_3-produced materials. It

is possible that this may play a role in charge separation and prevention of electron hole recombination. In any case it seems that the more ordered rod structures produced using the AC technique are preferable in terms of activity to the less elongated materials formed during the HNO_3 condensation.

Another possible rationale for these different catalytic activities might revolve around the preferential growth of the rutile rods along particular crystallographic axes leading to the preferential exposure of specific crystal faces [66]. These in turn might have higher conductivity or more favourable charge separation characteristics and therefore act as more active photo-catalysts [67].

In particular Penn *et al*. [66] initially discussed TiO_2 crystal growth in acidic solutions and show that a driving force involving the reduction in surface energy (and subsequent minimization of the area of high surface energy faces) resulted in the formation of distinctly faceted crystallites dominated by {101} surfaces.

Since this, several authors [67-69] have suggested that the differently exposed crystal faces can in fact have significantly different photocatalytic reactivity. It is possible that such a mechanism operates here where crystal growth is prohibited in certain directions, (due to the presence of the melamine borate salt within the acidic condensing mixture) allowing growth in other directions and therefore preferential exposure of more catalytically active crystal faces.

Conclusions

In contrast to the situation where C-doped anatase TiO_2 is produced, the addition of melamine borate to a condensing sol of TiO_2 precursor material (under acidic conditions where the sol is directed to form the rutile phase) does not result in the material formed having a decreased bandgap (as confirmed by UV-Vis spectroscopy) or the incorporation of dopant levels of C into the TiO_2 lattice (as confirmed by XPS measurements) and as yet there is no wet-chemistry method to reproducibly introduce C-dopants into a rutile TiO_2 nanoparticle lattice.

The presence of melamine borate (notwithstanding that it does not result in C-doping within the TiO_2 lattice) does affect the nature of the rutile produced, in that the crystals formed have a higher proportion or rutile phase (100%), increased surface areas and more defined rod-shaped morphologies than crystals which condensed in the absence of the melamine additive.

These larger surface areas and more defined crystals yield catalysts which have higher photo-catalytic activity than the analogous materials prepared in the absence of melamine borate.
So our attempts to produce C-doped rutile phase TiO_2 were unsuccessful. However, serendipitously we have come to a procedure for production of a more phase pure and more photo-reactive rutile phase.

Acknowledgements

We acknowledge and thank Science Foundation Ireland for their funding of this Strategic Research Cluster Programme (07/SRC/B1160) and our Industry Partners for their support of this Cluster. We specifically thank SSE Renewables for their support of E.M.N. We are also

grateful to Anne-Katrin Prescher for assistance with TOC analysis. We also thank the Erasmus exchange programme for providing funding to J.Z. to visit UCD. KRT acknowledges also the support received under the SFI-Airtricity-Stokes Professorship grant.

References

1. D. Macwan, P. N. Dave and S. Chaturvedi, *Journal of Materials Science*, 2011, **46**, 3669-3686.
2. A. Fujishima, T. N. Rao and D. A. Tryk, *Journal of Photochemistry and Photobiology C: Photochemistry Reviews*, 2000, **1**, 1-21.
3. J. M. Herrmann, *Catalysis Today*, 1999, **53**, 115-129.
4. M. R. Hoffmann, S. T. Martin, W. Y. Choi and D. W. Bahnemann, *Chemical Reviews*, 1995, **95**, 69-96.
5. Y. Paz, Z. Luo, L. Rabenberg and A. Heller, *Journal of Materials Research*, 1995, **10**, 2842-2848.
6. M. Ni, M. K. H. Leung, D. Y. C. Leung and K. Sumathy, *Renewable & Sustainable Energy Reviews*, 2007, **11**, 401-425.
7. M. Ashokkumar, *International Journal of Hydrogen Energy*, 1998, **23**, 427-438.
8. A. Mills and S. LeHunte, *Journal of Photochemistry and Photobiology A: Chemistry*, 1997, **108**, 1-35.
9. A. L. Linsebigler, G. Lu and J. T. Yates Jr, *Chemical Reviews*, 1995, **95**, 735-758.
10. N. Serpone, D. Lawless, R. Khairutdinov and E. Pelizzetti, *The Journal of Physical Chemistry*, 1995, **99**, 16655-16661.
11. B. Ohtani, S. W. Zhang, J. Handa, H. Kajiwara, S. Nishimoto and T. Kagiya, *Journal of Photochemistry and Photobiology A: Chemistry*, 1992, **64**, 223-230.
12. P. I. Gouma and M. J. Mills, *Journal of the American Ceramic Society*, 2001, **84**, 619-622.
13. G. Liu, X. Wang, Z. Chen, H. M. Cheng and G. Q. M. Lu, *Journal of Colloid and Interface Science*, 2009, **329**, 331-338.
14. S. Valencia, J. M. Marín and G. Restrepo, *Open Materials Science Journal*, 2010, **4**, 9-14.
15. W. Y. Choi, A. Termin and M. R. Hoffmann, *Angewandte Chemie-International Edition in English*, 1994, **33**, 1091-1092.
16. H. Irie, Y. Watanabe and K. Hashimoto, *The Journal of Physical Chemistry B*, 2003, **107**, 5483-5486.
17. M.J. Mattle, K. R.Thampi, *Applied Catalysis B: Environmental*, 2013, **140–141**, 348-355.
18. S. U. M. Khan, M. Al-Shahry and W. B. Ingler, *Science*, 2002, **297**, 2243-2245.
19. O. Lorret, D. Francova, G. Waldner and N. Stelzer, *Applied Catalysis B: Environmental*, 2009, **91**, 39-46.
20. R. Nakamura, T. Tanaka and Y. Nakato, *The Journal of Physical Chemistry B*, 2004, **108**, 10617-10620.
21. Y. Park, W. Kim, H. Park, T. Tachikawa, T. Majima and W. Choi, *Applied Catalysis B: Environmental*, 2009, **91**, 355-361.

22. S. Sakthivel, M. Janczarek and H. Kisch, *The Journal of Physical Chemistry B*, 2004, **108**, 19384-19387.
23. X. Z. Shen, J. Guo, Z. C. Liu and S. M. Xie, *Applied Surface Science*, 2008, **254**, 4726-4731.
24. T. Tachikawa, S. Tojo, K. Kawai, M. Endo, M. Fujitsuka, T. Ohno, K. Nishijima, Z. Miyamoto and T. Majima, *The Journal of Physical Chemistry B*, 2004, **108**, 19299-19306.
25. C. Y. Wang, D. W. Bahnemann and J. K. Dohrmann, *Chemical Communications*, 2000, 1539-1540.
26. T. Ikeda, T. Nomoto, K. Eda, Y. Mizutani, H. Kato, A. Kudo and H. Onishi, *The Journal of Physical Chemistry C*, 2008, **112**, 1167-1173.
27. R. Asahi, T. Morikawa, T. Ohwaki, K. Aoki and Y. Taga, *Science*, 2001, **293**, 269-271.
28. J.M. Herrmann, *New Journal of Chemistry*, (2012) 36, 4, 883-890.
29. E. M. Neville, M. J. Mattle, D. Loughrey, B. Rajesh, M. Rahman, J. M. D. MacElroy, J. A. Sullivan and K. R. Thampi, *The Journal of Physical Chemistry C*, 2012, **116**, 16511–16521.
30. J.A. Sullivan, K.R. Thampi, E.M. Neville and J.D. MacElroy, *Journal of Photochemistry and Photobiology A: Chemistry*, (2013), **267**, 17-24.
31. C. Y. Jimmy, J. Yu, W. Ho, Z. Jiang and L. Zhang, *Chemistry of Materials*, 2002, **14**, 3808-3816.
32. V. Stengl, T. M. Grygar, F. Opluštil and T. Němec, *Journal of Hazardous Materials*, 2012, **227**, 62.
33. A. Zaleska. *Recent Patents on Engineering* (2008), 2, 157-164
34. M.Pelaez, N.T. Nolan, S.C. Pillai, M.K. Seery, P.Falaras, A.G. Kontos, P.S.M. Dunlop, J.W.J. Hamilton, J.A.Byrne, K.O'Shea, M.H. Entezari, D.D. Dionysiou, *Applied Catalysis B: Environmental,* (2012), 125, 1, 331-349
35. D. Dvoranova, V. Brezova, M. Mazur, M.A. Malati, Applied Catalysis B: Environmental, 37, 2, 2002, 91-105
36. X. Yang, J.Chen, L.Gong, M. Wu, J.C. Yu. Journal of the American Chemical Society, 2009, 131 (34), 12048-12049, 2009.
37. H. Kamisaka, T. Adachi, and K. Yamashita J. Chem. Phys. 123, 084704 (2005)
38. D. Reyes-Coronado, G. Rodríguez-Gattorno, M. E. Espinosa-Pesqueira, C. Cab, R. de Coss and G. Oskam, *Nanotechnology*, 2008, **19**, 145605-145614.
39. G. Oskam, A. Nellore, R. L. Penn and P. C. Searson, *The Journal of Physical Chemistry B*, 2003, **107**, 1734-1738.
40. A. Navrotsky, *Geochemical Transactions*, 2003, **4**, 34-37.
41. J. Ovenstone and K. Yanagisawa, *Chemistry of Materials*, 1999, **11**, 2770-2774.
42. H. Cheng, J. Ma, Z. Zhao and L. Qi, *Chemistry of Materials*, 1995, **7**, 663-671.
43. Y. Li, Y. Fan and Y. Chen, *Journal of Materials Chemistry*, 2002, **12**, 1387-1390.
44. M. N. Tahir, P. Theato, P. Oberle, G. Melnyk, S. Faiss, U. Kolb, A. Janshoff, M. Stepputat and W. Tremel, *Langmuir*, 2006, **22**, 5209-5212.
45. Z. Tang, J. Zhang, Z. Cheng and Z. Zhang, *Materials Chemistry and Physics*, 2002, **77**, 314-317.
46. J. Livage, *Sol--Gel Science and Technology*, 1989, 103-152.
47. M. Gopal, W. Moberly Chan and L. De Jonghe, *Journal of Materials Science*, 1997, **32**, 6001-6008.
48. P. Wang, S. M. Zakeeruddin, P. Comte, R. Charvet, R. Humphry-Baker and M. Grätzel, *The Journal of Physical Chemistry B*, 2003, **107**, 14336-14341.
49. C. C. Wang and J. Y. Ying, *Chemistry of Materials*, 1999, **11**, 3113-3120.

50. H. Yin, Y. Wada, T. Kitamura, S. Kambe, S. Murasawa, H. Mori, T. Sakata and S. Yanagida, *Journal of Materials Chemistry*, 2001, **11**, 1694-1703.
51. F. Dachille, P. Simons and R. Roy, *American Mineralogist*, 1968, **53**, 1929-1939.
52. R. Nicula, M. Stir, C. Schick and E. Burkel, *Thermochimica Acta*, 2003, **403**, 129-136.
53. A. N. MerrsEws and J. Israel, *American Mineralogist*, 1976, **61**, 419424.
54. R. A. Spurr and H. Myers, *Analytical Chemistry*, 1957, **29**, 760-762.
55. R. Shirley, M. Kraft and O. R. Inderwildi, *Physical Review B*, 2010, **81**, 075111.
56. A. L. Patterson, *Phys. Rev.*, 1939, **56**, 978–982.
57. D. Singh, N. Singh, S. D. Sharma, C. Kant, C. Sharma, R. Pandey and K. Saini, *Journal of sol-gel science and technology*, 2011, **58**, 269-276.
58. J. I. Pankove, *Optical processes in semiconductors*, Dover Publications, 1971.
59. E. Papirer, R. Lacroix, J. B. Donnet, G. Nanse and P. Fioux, *Carbon*, 1995, **33**, 63-72.
60. T. Ohno, T. Tsubota, K. Nishijima and Z. Miyamoto, *Chemistry Letters*, 2004, **33**, 750-751.
61. W. J. Ren, Z. H. Ai, F. L. Jia, L. Z. Zhang, X. X. Fan and Z. G. Zou, *Applied Catalysis B-Environmental*, 2007, **69**, 138-144.
62. S. Sakthivel and H. Kisch, *Angewandte Chemie-International Edition*, 2003, **42**, 4908-4911.
63. Q. Xiang, J. Yu and P. K. Wong, *Journal of Colloid and Interface Science*, 2011, **357**, 163-167.
64. C. Ribeiro, C. Vila, Daniel B. Stroppa, V.R. Mastelaro, J. Bettini, E. Longo, and E. R. Leite. *J. Phys. Chem. C* 2007, **111**, 5871-5875.
65. C. Coughlan, A. Singh and K.M. Ryan, *Chem. Mater.* 2013, **25**, 653−661.
66. R.L. Penn and J.F. Banfield, *Geochimica et Cosmochimica Acta*, **63**, 10, (1999), 1549 –1557.
67. N. Murakami, S. Katayama, M. Nakamura, T. Tsubota, and T. Ohno, *J. Phys. Chem. C, (*2011), *115,* 419–424
68. T. Ohno, K. Sarukawa, M. Matsumura, *New Journal of Chemistry,*(2002), **26**, 1167-1170.